



The topology of fMRI-based networks defines the performance of a graph neural network for the classification of patients with major depressive disorder

Elena N. Pitsik^{a,b}, Vladimir A. Maximenko^{a,b}, Semen A. Kurkin^{a,b}, Alexander P. Sergeev^a, Drozdostoy Stoyanov^c, Rositsa Paunova^c, Sevdalina Kandilarova^c, Denitsa Simeonova^c, Alexander E. Hramov^{a,b,*}

^a Engineering School of Information Technologies, Telecommunications and Control Systems, Ural Federal University, Mira str., 19, Ekaterinburg, 620002, Russia

^b Baltic Center of Neurotechnology and Artificial Intelligence, Immanuel Kant Baltic Federal University, 14 A. Nevskogo ul., Kaliningrad, 236016, Russia

^c Department of Psychiatry and Medical Psychology, Research Institute, Medical University of Plovdiv, 15A Vassil Aprilov Blvd., Plovdiv, 4002, Bulgaria

ARTICLE INFO

Keywords:

Graph neural network
Thresholding
fMRI
Topology analysis
GNN interpretation
Major depression disorder

ABSTRACT

Deep learning approaches are state-of-the-art computational tools employed at analyzing big data in fundamental and applied science. Recently, they gained popularity in neuroscience and medicine due to their ability to recognize hidden patterns and nonlinear relations in large amounts of nonstationary and ambiguous neuroimaging biomedical data. Analysis of functional connectivity matrices is a perfect example of such a computational task assigned to deep learning. Here, we trained a graph neural network (GNN) to classify the major depressive disorder (MDD) based on the topological features of the brain functional connectivity identified using fMRI technology. We show that the most important feature of the functional brain network is the shortest path, which defines the optimal number of GNN layers to ensure the most accurate classification in patients with MDD. The proposed GNN-based classifier reaches an accuracy of 93%, which is in line with the achievements of the best connectivity-based classifiers for MDD. The maximal F1-score is observed when we input the sparse graph consisting of 2.5% of the connections of the original one, which avoids feeding large amounts of data to the GNN and reduces overfitting.

1. Introduction

Functional connectivity (FC) of the brain refers to statistical dependence between measures of temporal neuronal activity recorded from the spatially distributed regions of the brain [1–3]. Studies of functional brain networks are carried out non-invasively, with FC defined usually as the presence of the temporal correlation between time series of electrical activity or deoxygenated blood levels in distinct areas of the brain [4]. The first can be realized using electro- or magnetoencephalography (EEG/MEG), which reflects temporal dynamics of averaged post-synaptic potential and dendritic currents of local neural ensembles and, hence, provide a direct measurement of neural activity on the macroscopic level [5]. The second approach uses functional MRI (fMRI) and blood-oxygen-level dependent (BOLD) signals that reflect temporal changes in the metabolic demand, providing an indirect measurement of this neural functioning [6]. While the first approach allows for the analysis of fast changes in functional connectivity, e.g., during

stimulus processing, but with low spatial resolution, the second method does not allow to analyze of rapid neuronal activity changes due to the MRI features of brain metabolic registration but provides high spatial localization of FC between distant regions of the brain. In the latter case, therefore, the analysis of FC in the resting-state condition is of particular interest, reflecting the slow dynamics of brain activity in the form of resting-state networks [7–9].

Studying functional brain networks, including resting-state networks, is of particular interest for diagnosing various neurophysiological disorders. FC measurements are highly effective in diagnosing schizophrenia, bipolar disorder, autism spectrum disorder, and attention deficit hyperactivity disorder, as well as major depressive disorder (MDD). The latter is a leading cause of disability worldwide [10]. The exact pathophysiological mechanisms of MDD remain unclear. Symptoms of a depressive episode include anhedonia, insomnia, sadness, anxiety, and suicidal ideation [11]. In addition, the condition

* Corresponding author at: Baltic Center of Neurotechnology and Artificial Intelligence, Immanuel Kant Baltic Federal University, 14 A. Nevskogo ul., Kaliningrad, 236016, Russia.

E-mail address: hramovae@gmail.com (A.E. Hramov).

<https://doi.org/10.1016/j.chaos.2022.113041>

Received 16 November 2022; Accepted 19 December 2022

Available online 2 January 2023

0960-0779/© 2022 Elsevier Ltd. All rights reserved.

is characterized by impaired cognitive and emotional processing of information [12]. For this reason, considerable research effort has focused on the neurobiological underpinnings that support emotion processing and mood regulation, which are affected in patients with depressive disorder [13]. A large number of studies aim to explain brain abnormalities in depressive disorders based on FC methodology [14]. Based on the variety of methods proposed to measure FC among brain regions using fMRI [15], it has been shown that the brain networks that are taught to be involved in MDD are the default mode network, executive control network, and salience network [16–18]. However, other brain regions also participate in pathological changes in FC. For example, decreased thalamic connectivity with the salience network was reported in patients with MDD [16].

However, the restoration of functional brain networks is only the first, already well-studied stage of the analysis of the functional integration of the brain. In the second stage, we should use mathematical methods of graph-based data analysis to provide potential biomarkers for classifying or predicting brain disorders. Feature extraction from a large amount of FC measures as a biomarker for building a model to classify brain disorders is an important and challenging problem at the interface between complex network theory, machine learning, and biomedicine [15]. Among the commonly used feature selection methods in classification strategies in fMRI FC are the filter-based method [19], where feature selection is independent of classifier/model building, and the wrapper methods [20], which involve optimizing classifiers as part of the feature selection. Embedded mathematical approaches [21], which combine classification and feature selection into a single decision-making process, have also been applied to the classification of FC data. At the same time, more interpretable approaches can also show high efficiency. In our work [22], traditional characteristics of complex networks, such as clustering coefficient, eigenvector centrality, and node strength, were used to classify the FC data of a patient with MDD. Based on these network measures, significant differences in FC between depressed patients and healthy controls were demonstrated, with linear discriminant analysis (LDA) demonstrated to be highly accurate in differentiating between depressed and healthy subjects. Along with LDA, the support vector machine (SVM), which is a commonly used model in supervised learning, is widely used to classify selected features.

Recently, deep learning (DL) has attracted increasing interest in various areas and also has been applied in the classification of brain disorders. In contrast to traditional machine learning methods, DL methods are capable of learning the optimal representation directly from the raw data, in our case, from the obtained fMRI-based correlation matrices [15,23,24]. The DL approach is based on the nonlinear transformation of the raw data through many layers, and the DL nonlinear model provides hidden features with higher levels of abstraction. It leads to automatically solving difficulties in the feature selection, especially when the dimension of features is too large or when there is limited prior knowledge about the analyzed dataset. As a consequence, artificial neural networks (ANNs) are often used to build classifiers of patients using fMRI data [25,26]. In this case, ANN learns to identify subjects with brain disorders by analyzing training datasets, including both healthy and disordered persons, and using this information to classify new subjects. As noted in the Review [15], an auto-encoder is a type of ANN widely used for brain disorders classifications based on fMRI data. The deep belief network is another class of ANN for the classification of brain disorders using fMRI data.

However, in the last few years, a new class of DL methods, the so-called graph neural networks (GNNs), has been actively developed to perform inference on data described by graphs [27]. GNNs are the ANNs that can be directly applied to process data that can be represented as graphs and provide an easy way to do node-level, edge-level, and graph-level classification and prediction tasks [28,29]. At present, several applications in various fields have been solved using GNNs, e.g., protein interface prediction [30], breast cancer subtype

classification [31], chemical reaction prediction [32], cognitive processes in subject–subject interaction [33], modeling of various physical systems [34,35], etc. (a detailed overview of the GNN applications can be found in [29]). We believe that this new machine learning tool can be effective in analyzing functional brain networks and allow the classification of various neurological diseases based on the topological features of the brain FC identified using fMRI technology. Our approach is an explorative, data-driven study aiming to investigate newer approaches to classify features of brain FC in terms of its topology using the GNN approach. We focus in this study on analyzing the performance of the GNN-based classifier of MDD patients as a function of the topology of the fMRI-based functional brain network. We show that the most important feature of the functional brain network is the shortest path, which specifies the optimal number of GNN layers to ensure the most accurate classification in patients with MDD.

2. Methods

2.1. fMRI dataset

2.1.1. Subjects

The dataset included fMRI data from 84 subjects: 49 healthy controls (Control group) and 35 patients with a major depressive disorder (MDD group). Subjects having a previous history of comorbid psychiatric conditions, autoimmune diseases, neurological diseases, history of head trauma, or any metal implants in-compatible with the MRI were excluded. All participants provided a written consent form complying with the Declaration of Helsinki. The study was approved by the Medical University of Plovdiv Ethical Committee (2/19 April 2018).

2.1.2. MRI scanning

The MRI scanning procedure was performed on a 3T MRI system (GE Discovery 750w, General Electric, BostonMA, USA). The protocol included a high-resolution structural scan (Sag 3D T1) with slice thickness of 1 mm, matrix 256×256 , TR (relaxation time) 7.2 s, TE (echo time) 2.3 s, and flip angle 12° , FOV 24, 368 slices and resting-state functional scan—2D echo-planar imaging (EPI) with slice thickness 3 mm, matrix 64×64 , TR 2000 ms, TE 30 ms, 36 slices, flip angle 90° , FOV 24, a total of 192 volumes. Before the EPI sequence, subjects were instructed to remain as still as possible with their eyes closed and not to think of anything in particular (see Fig. 1A). Duration time of the resting-state functional scan was 6 min.

2.1.3. FMRI data processing

Neuroimaging data were processed using SPM 12 software (Statistical Parametric Mapping) running on MATLAB R2021 for Windows. The functional images of each participant were first realigned, co-registered with the high-resolution anatomical image, and normalized to standard MNI space. Parameters for the realignment step were the following: quality 0.9, separation 4, smoothing FWHM 5, 2nd degree B-spline interpolation, no wrap, 12×12 basis function, regularization 1 with medium factor, without Jacobian deformations, 5 iterations, average Taylor expansion point. The co-registration method was set to the normalized mutual information with the following parameters: separation [4 2], tolerances [0.02 0.02 0.02 0.001 0.001 0.001 0.01 0.01 0.01 0.001 0.001 0.001], histogram smoothing [7 7]. MNI normalization parameters were the following: bias regularization 0.0001, bias FWHM 60 mm cutoff, affine regularization ICBM European brain template, warping regularization [0 0.001 0.5 0.05 0.2], no smoothing, sampling distance 3.

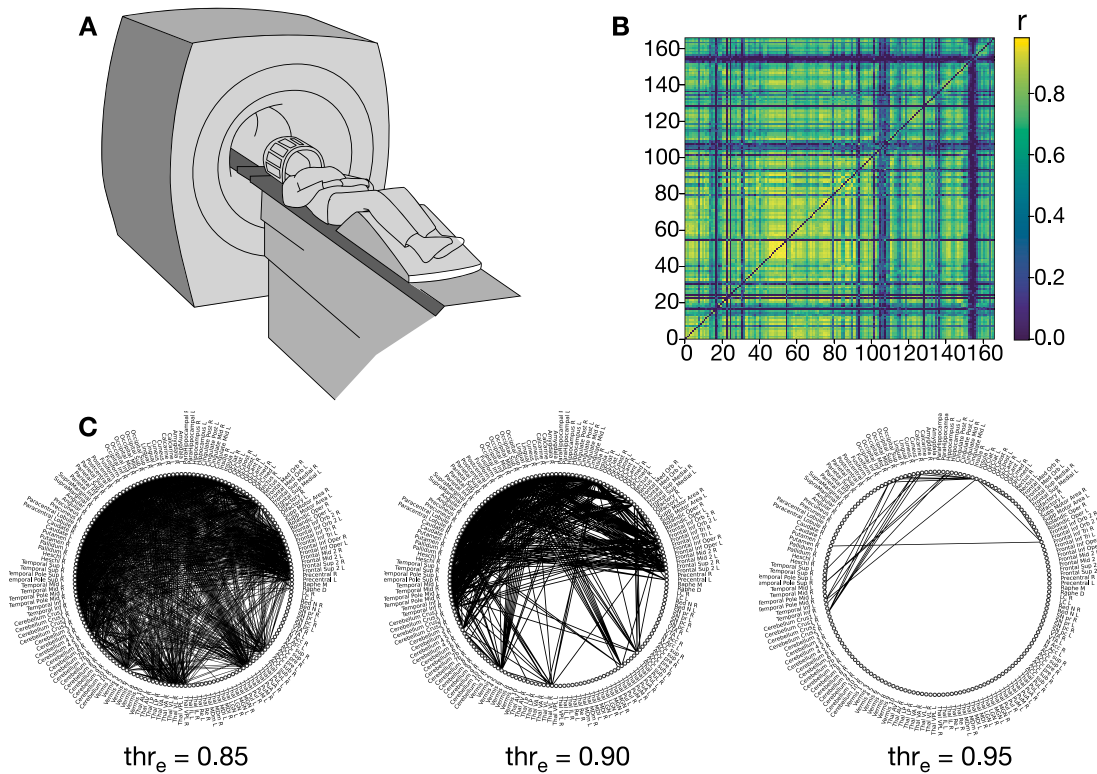


Fig. 1. Schematic representation of the dataset extraction. **A** – experimental process of BOLD time series recording during fMRI. **B** – example of correlation matrix for one subject from the control group. **C** – examples of the circular connectivity plot of the same correlation matrix, thresholded with different thr_e .

2.1.4. Connectivity matrix calculation

The normalized functional MRI volumes extracted with the help of SPM 12 were parcellated into 166 regions according to the automated anatomical labeling atlas AAL3 [36]. To estimate the connectivity between the regions of interest, we calculated an average BOLD time series $x_i(t)$ (across the voxels in each parcellation (i) and Pearson correlation coefficients for all pairs of the mean parcellation activities. The Pearson correlation coefficient measures the linear relationship between two random variables and is good for low-frequency processes as fMRI signals [37]. Connectivity matrix calculation from the averaged activity time-series was performed with the help of Matlab statistics “corrcoef” function. Thus, we obtained for each subject a 166×166 symmetric connectivity matrix R . Each cell of the connectivity matrix ($r_{i,j}$) represents the strength of the connection (or edge) between two parcels:

$$r_{i,j} = \frac{\sum_{k=1}^n (x_{i,k} - \bar{x}_i)(x_{j,k} - \bar{x}_j)}{\sqrt{\sum_{k=1}^n (x_{i,k} - \bar{x}_i)^2 \sum_{k=1}^n (x_{j,k} - \bar{x}_j)^2}}. \quad (1)$$

Here, n is the length of the x time-series, and \bar{x} is the mean of the x time-series. An example of the correlation matrix for single subject from Control group is presented on Fig. 1B.

2.2. Thresholding

Our dataset consists of several relatively large structures, representing summarized activity in the form of correlation matrices. Such networks are very difficult to analyze due to the large number of connections that make it impossible to see any structure. In this case, a common choice is to discard the least significant connections by applying some threshold and study the sparser network instead [38]. Although existing literature indicates that such an approach can lead to the loss of the important features critical for understanding the system, we believe that thresholding is convenient in the framework of understanding the message-passing mechanism of the graph convolutional network (GCN) blocks.

We applied 20 thresholds thr_e to the edge weights in range from 0.0 to 0.95 with step 0.05 and binarized the resulting matrix. As a result, we discarded the less important connections based on the thr_e value, leaving only the edges with the strongest Pearson’s coefficient values. An example of a thresholding procedure for a single subject is presented in Fig. 1C, which also illustrates the necessity of the thresholding procedure: we can see that, even with one of the highest $thr_e = 0.85$, the structural features of the network cannot be highlighted. The whole process is schematically shown in Fig. 2A. We proceeded with analyzing the topologies of the networks by applying linear regression to the corresponding degree distributions. Fig. 3 shows the results for each threshold, including the initial network.

2.3. Shortest paths analysis

Since the goal of the research was to provide a correlation between the GNN performance and topological features of the data, we considered the shortest paths as a possible indicator. In our opinion, the differences between shortest path distributions for two considered classes can help to explain the results of classification. Therefore, for each thr_e , we obtained the shortest path distributions for both groups of subjects, and checked its dependence from thr_e (see Fig. 4B). Then, for each distribution, we calculated the value d^* – the length of the shortest path with the maximum t-statistic value based on the t-test for independent samples with the correction to the multiple comparisons problem. We used this parameter to monitor the changes of differences in topological properties of two considered classes, as well as to establish the possible correlations between the shortest path distributions and GNN performance.

2.4. Graph neural network

We used a dataset of 84 correlation matrices obtained from resting state fMRI (rs-fMRI) data of people with major depression disorder

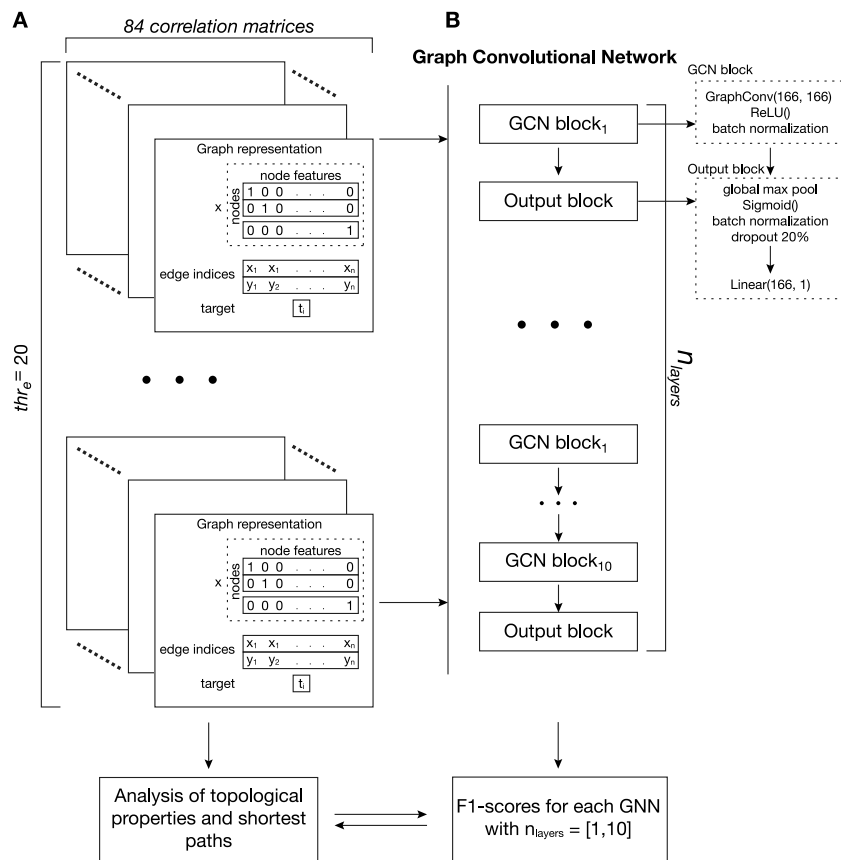


Fig. 2. Schematic representation of the research. **A** – to each graph from the initial dataset, we applied the threshold thr_e to discard the less important edges and study the corresponding topological changes, as well as the reaction of GNN on them. Each graph was represented in COO format with parameters x , $edge\ indices$ and y ; **B** – each thr_e -dataset was fed to the GNN with different number of graph convolutional network (GCN) blocks to compare the results with topological properties of the networks. Each GNN model had n_{layers} GCN blocks, where $n_{layers} = [1, 10]$.

(MDD) and healthy control (Control) individuals (49 Control and 35 MDD). For this research, we used only a positive subnetwork consisting of connections with positive Pearson correlation coefficients.

For GNN training, each graph in the dataset was organized in the Coordinate (COO) format, as shown in Fig. 2A. The set x corresponds to node features. Since each node in the correlation matrix represents one region of interest, we created a 166×166 binary diagonal matrix, where the first dimension corresponds to the nodes and the second dimension — to the features, stating that each node is unique and has a separate feature, without specifying the nature of the feature.

The set $edge\ indices$ is a 2D array containing the edges in COO format, with the elements in the first and the second row containing indices of outgoing and incoming nodes, respectively. Finally, a single-element array $target$ contained the label of the current graph, which in our binary classification task was either 0 or 1. Label 0 was assigned for MDD class, and label 1 was for the Control class.

We calculated the performance of 10 GNN models, increasing the number of GCN blocks ($n_{layers} = [1, 10]$) to check the possible correlation between the depth of the model and the topological features of the dataset. One GCN block consisted of one graph convolutional layer for feature extraction, ReLU() activation function, and batch normalization. We also added one pool layer to reduce dimensionality and one dense layer as final classifiers. The architecture of the model is illustrated in Fig. 2B.

The hyperparameters of the model were chosen as follows:

- (1) Learning rate = 0.0005;
- (2) 166 hidden neurons on all layers;
- (3) Adam optimizer;
- (4) Binary cross entropy with logits as loss function;

(5) Batch size = 32;

(6) Dropout 20%;

(7) 100 epochs.

The dataset used for classification experiments is relatively small and unbalanced, therefore we applied a couple of precautionary procedures to prevent overfitting. In particular, we performed training and testing with a Stratified k-fold with 10 folds to ensure the balanced representation of each class and to test the model on several different subsets of test data. To evaluate the model performance, we monitored F1-score. For each thr_e , we calculated the value max_{GCN} that equals the parameter n_{layers} , for which the F1-score of the corresponding GNN model was the largest.

3. Results

3.1. Topology analysis

After applying thresholding, we analyzed the topological properties of graphs by calculating the degree distribution with linear regression. As Fig. 3 shows, the topology of the networks for both classes changes from random-like distribution (upper row) to a scale-free network (lower row). Here, the parameter x_1 , shown in figures for each class, is a directional indicator representing an angle of linear regression. For $thr_e = 0.95$, $x_1 = -2.07$ for the Control group, suggesting that the topology of the rs-fMRI functional connectivity network with the strongest links becomes fully scale-free in healthy subjects but not in MDD patients ($x_1 = -1.85$).

Next, we calculated for each thr_e the shortest path distribution for the paths of length $d = [2, 10]$, where d is the number of nodes

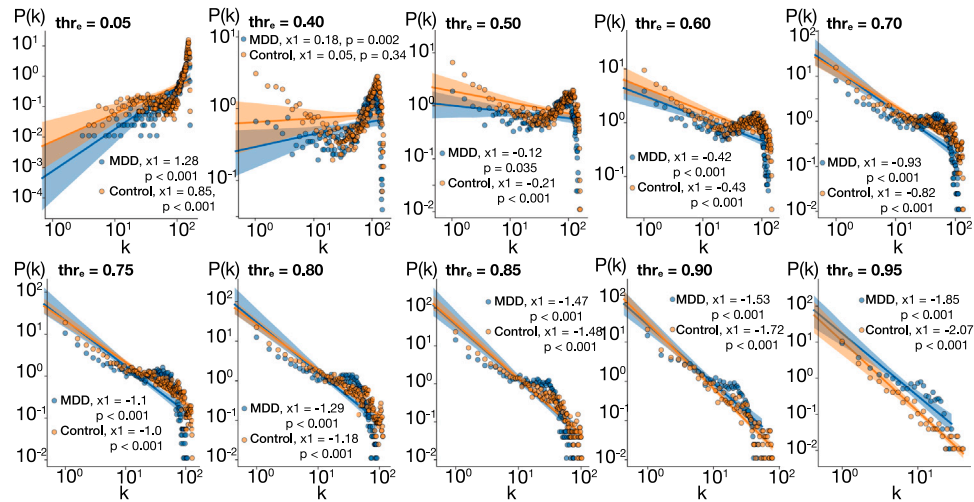


Fig. 3. Degree distributions of networks corresponding to each thr_e value with linear regression. Each figure shows degree distributions for two groups of subjects (blue — MDD group, orange — Control group). Parameter $x1$ is an angle indicator; p is a p -value of linear regression. (For interpretation of the references to color in this figure legend, the reader is referred to the web version of this article.)

Table 1
Detailed results of topological analysis and GNN performance for each thr_e .

thr_e	d^*	max_{GCN}	F1-score
0.0	3	1	88.38
0.05	3	3	89.63
0.10	3	2	87.88
0.15	3	2	87.62
0.20	3	2	86.21
0.25	3	2	86.57
0.30	3	2	87.6
0.35	3	2	93.24
0.40	3	2	90.4
0.45	3	3	88.38
0.50	3	3	92.88
0.55	3	2	91.71
0.60	3	2	86.81
0.65	3	2	85.57
0.70	4	3	89.24
0.75	4	10	84.29
0.80	5	9	87.14
0.85	5	8	87.4
0.90	6	5	94.6
0.95	2	5	84.66

in the corresponding paths. In Fig. 4A, we show the mean circular connectivity plots for both groups with only those edges that form the shortest paths of lengths $d = 4$ and $d = 5$ (left and right panels, respectively). We used networks thresholded at $thr_e = 0.95$ for these illustrations. One can see that, despite a large number of connections, the pattern of connectivity is rather different in the two groups. To explore the dependence of these differences from thr_e , we applied the t-test for independent samples to the shortest path distributions. Results are shown in Fig. 4B, where the white area highlights the maximum values of t-statistic with the corresponding $p_{val} < 0.05$, and d^* is the length of the shortest path, for which the differences between the groups are most pronounced. Detailization of the d^* for each thr_e is provided in Table 1. Fig. 4B shows that an increase of the thr_e leads to the formation of a larger amount of shortest paths of length $d > 2$ in the MDD group compared with Control. The maximum value of $thr_e = 0.95$ corresponds to the $d^* = 2$, which indicates the deterioration of long-path structures in the MDD group, also confirmed by the shape of the corresponding distribution (Fig. 3, lower right).

3.2. GNN-based classification

In the previous subsection, we considered the topological changes in analyzed networks induced by the thresholding procedure. To see the correlation between these results and GNN performance, we conducted a numerical experiment consisting of feeding datasets with different thr_e to GNN models of different architecture. In particular, we designed 10 GNN models with a different number of GCN blocks to check the dependence of performance on the topological features of the data. The results of the F1-score for each (model, thr_e)-pair are shown in Fig. 4C. Here, the white line corresponds to the maximum F1-score for each number of layers. The corresponding values of number of layers — max_{GCN} — are detailed in Table 1. First, one can see that max_{GCN} increases with thr_e . Second, the shape of the F1-score increase in Fig. 4C is qualitatively similar to the shape of the t-statistic increase in Fig. 4B, which indicates the possible correlation between d^* and max_{GCN} . To check this, we applied linear regression to show the relationships between the graphs' topology and corresponding GNN performance more clearly (see Fig. 4D). Here, we demonstrate the obvious uptrend, evidencing that the optimal depth of the GNN model indeed correlates with the statistical parameter based on shortest path distribution. Moreover, the estimation of the relationships between two variables with Spearman correlation also shows an increasing trend between max_{GCN} and d^* ($r_s = 0.72$, $p_s = 0.00034$).

Finally, Fig. 5 illustrates our method's efficiency via receiver operating characteristic (ROC) curves. One can see that the model chosen by our approach based on shortest paths ("best performance") shows a higher AUC (area under the curve) score than the model with 1 GCN block, which we chose as a reference.

4. Discussion and conclusion

We have found that the optimal depth of GNN (the number of layers) depends on the topology of the analyzed graphs. The F1 score varies from 80% to 90% depending on the GNN depth. When the graph is fully connected, F1 is maximal for the 1-layer GNN and decreases if the number of layers grows. For large thresholds, the graphs become sparse and 1-layer GNN fails to learn their topology. Thus, the F1 score grows reaching the maximal value at a certain (optimal) depth. Again, further increase in depth causes F1 reduction. We used cross-validated F1 score; therefore, it might decline due to underfitting and overfitting issues. Thus, we concluded that for the fully connected graph, one layer is enough to learn the graph topology, whereas more layers

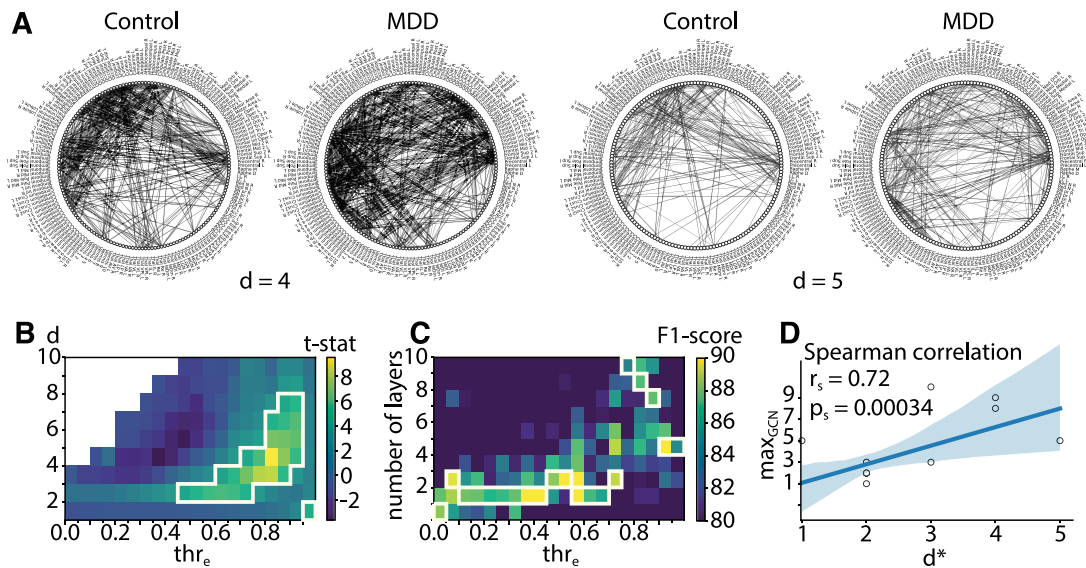


Fig. 4. A – circular connectivity plots for both groups, on which each edge is included into the shortest path of length $d = 4$ (left) or $d = 5$ (right). B – dependence of t-statistic of shortest path distribution between MDD and Control on thr_e . Here, the white line indicates the maximum values of t-statistic with corresponding $p_{val} < 0.05$. C – results testing the dependence of GNN with different depths on thr_e . The white line highlights the maximum F1-score for each model configuration (*number of layers* parameter). D – correlation between GNN depth with the highest performance (Max_{GCN}) and the length of shortest path with the most pronounced difference between the two classes (d^*). The relationships between variables are approximated with linear regression with a confidence interval of 0.95 and measured with Spearman’s correlation.

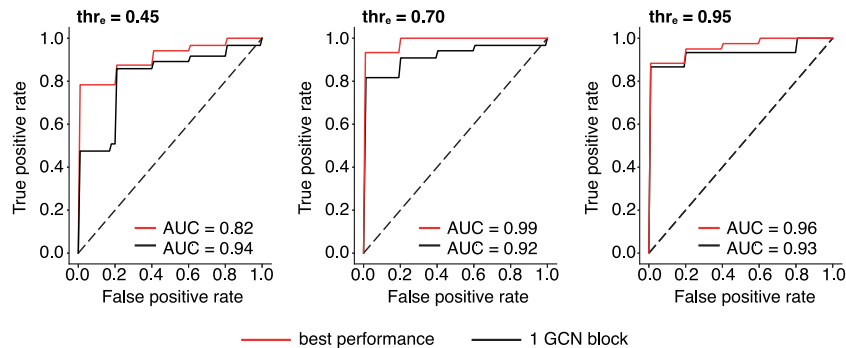


Fig. 5. ROC curves for three $thr_e = [0.45, 0.70, 0.95]$ for two cases: GNN model with 1 GCN block (black curve) and GNN model with best performance (red curve). The number of GCN blocks for models with the best performance for each thr_e is detailed in Table 1. (For interpretation of the references to color in this figure legend, the reader is referred to the web version of this article.)

cause overfitting. For the sparse topologies, growing depth reduces underfitting until it reaches an optimal value. Further increase in depth causes overfitting.

It is known that overfitting of the deep GNN may be caused by over-smoothing [39]. An intuitive notion of over-smoothing is that the mixture of neighborhood features by graph convolution drives the output of an infinitely-deep GNN towards a space that contains limited distinguished information between nodes. Thus, over-smoothing erases important discriminative information from the input, leading to poor trainability [40].

We report the positive correlation between the optimal depth and the length of the shortest path in the graphs. The shortest path is the minimal number of links connecting the pair of nodes. Following the concept of GNN, once the nodes are connected, their representation on the layers will be similar due to shared neighbors. This is exactly what over-smoothing means. Thus, we suppose that the shortest path defines a characteristic scale of the graph that affects GNN’s performance. On the layers whose number exceed the shortest path the majority of nodes lose their distinguished information.

Revealed correlation allows researchers to predefine a search space for an optimal depth before optimizing hyperparameters of GNN. It reduces computational time when dealing with big graph-structured data.

The proposed GNN-based classifier and the obtained results are also essential for clinical purposes due to the differentiating between depression patients and healthy individuals. Our classifier reached an accuracy of 93% (when the threshold value equals 0.15 and there are 2 layers in GNN). Such performance is in line with the achievements of the best connectivity-based classifiers for MDD. Earlier studies in this field focused mainly on specific regions and networks, and reached accuracy of around 90% [41]. Later, whole-brain connectivity analyses were prevalent, where the classification accuracy reached 90%–94% [22,42]. Some recent studies identified effective biomarkers for depression diagnosis using a fusion strategy of multiple resting-state connectivity measures (intrinsic, dynamic functional connectivity, effective connectivity) and achieved an accuracy of approximately 91% [43]. Remarkably, the proposed GNN shows the maximal F1-score when we input the sparse one consisting of 2.5% (on average) of the connections of the original graph (this corresponds to the threshold

value of 0.9). Thus, thresholding avoids feeding large amounts of data to the GNN and reduces overfitting.

Declaration of competing interest

The authors declare that they have no known competing financial interests or personal relationships that could have appeared to influence the work reported in this paper.

Data availability

Data will be made available on request.

Acknowledgments

The research funding from the Ministry of Science and Higher Education of the Russian Federation (Ural Federal University Program of Development within the Priority-2030 Program) is gratefully acknowledged.

References

- [1] Friston KJ. Functional and effective connectivity: a review. *Brain Connect* 2011;1(1):13–36.
- [2] Park H-J, Friston K. Structural and functional brain networks: from connections to cognition. *Science* 2013;342(6158):1238–41.
- [3] Hramov AE, Frolov NS, Maksimenko VA, Kurkin SA, Kazantsev VB, Pisarchik AN. Functional networks of the brain: from connectivity restoration to dynamic integration. *Phys-Usp* 2021;64(6):584.
- [4] Babaeeghazvini P, Rueda-Delgado LM, Gooijers J, Swinnen SP, Daffertshofer A. Brain structural and functional connectivity: A review of combined works of diffusion magnetic resonance imaging and electro-encephalography. *Front Hum Neurosci* 2021;585.
- [5] Sakkalis V. Review of advanced techniques for the estimation of brain connectivity measured with EEG/MEG. *Comput Biol Med* 2011;41(12):1110–7.
- [6] Rogers BP, Morgan VL, Newton AT, Gore JC. Assessing functional connectivity in the human brain by fMRI. *Magn Reson Imaging* 2007;25(10):1347–57.
- [7] Van Den Heuvel MP, Pol HEH. Exploring the brain network: a review on resting-state fMRI functional connectivity. *Eur Neuropsychopharmacol* 2010;20(8):519–34.
- [8] Lee MH, Smyser CD, Shimony JS. Resting-state fMRI: a review of methods and clinical applications. *Am J Neuroradiol* 2013;34(10):1866–72.
- [9] Zhang Y, Wu W, Toll RT, Naparstek S, Maron-Katz A, Watts M, et al. Identification of psychiatric disorder subtypes from functional connectivity patterns in resting-state electroencephalography. *Nat Biomed Eng* 2021;5(4):309–23.
- [10] Reddy M. Depression: the disorder and the burden. *Indian J Psychol Med* 2010;32(1):1–2.
- [11] Chen Z, Xia M, Zhao Y, Kuang W, Jia Z, Gong Q. Characteristics of intrinsic brain functional connectivity alterations in major depressive disorder patients with suicide behavior. *J Magn Reson Imaging* 2021;54(6):1867–75.
- [12] Gotlib IH, Joormann J. Cognition and depression: current status and future directions. *Ann Rev Clin Psychol* 2010;6:285.
- [13] Mulders PC, van Eijndhoven PF, Schene AH, Beckmann CF, Tendolkar I. Resting-state functional connectivity in major depressive disorder: a review. *Neurosci Biobehav Rev* 2015;56:330–44.
- [14] Kaiser RH, Andrews-Hanna JR, Wager TD, Pizzagalli DA. Large-scale network dysfunction in major depressive disorder: a meta-analysis of resting-state functional connectivity. *JAMA Psychiatry* 2015;72(6):603–11.
- [15] Du Y, Fu Z, Calhoun VD. Classification and prediction of brain disorders using functional connectivity: promising but challenging. *Front Neurosci* 2018;12:525.
- [16] Luo L, Wu H, Xu J, Chen F, Wu F, Wang C, et al. Abnormal large-scale resting-state functional networks in drug-free major depressive disorder. *Brain Imaging Behav* 2021;15(1):96–106.
- [17] Yang Y, Zhong N, Imamura K, Lu S, Li M, Zhou H, et al. Task and resting-state fMRI reveal altered salience responses to positive stimuli in patients with major depressive disorder. *PLoS One* 2016;11(5):e0155092.
- [18] Liang S, Deng W, Li X, Greenshaw AJ, Wang Q, Li M, et al. Biotypes of major depressive disorder: Neuroimaging evidence from resting-state default mode network patterns. *NeuroImage: Clin* 2020;28:102514.
- [19] Guyon I, Elisseeff A. An introduction to feature extraction. In: *Feature extraction*. Springer; 2006, p. 1–25.
- [20] Yu Y, Shen H, Zhang H, Zeng L-L, Xue Z, Hu D. Functional connectivity-based signatures of schizophrenia revealed by multiclass pattern analysis of resting-state fMRI from schizophrenic patients and their healthy siblings. *Biomed Eng Online* 2013;12(1):1–13.
- [21] Lal TN, Chapelle O, Schölkopf B. Combining a filter method with SVMs. In: *Feature extraction*. Springer; 2006, p. 439–45.
- [22] Stoyanov D, Khorev V, Paunova R, Kandilarova S, Simeonova D, Badarin A, et al. Resting-state functional connectivity impairment in patients with major depressive episode. *Int J Environ Res Public Health* 2022;19(21):14045.
- [23] Valliani AA-A, Ranti D, Oermann EK. Deep learning and neurology: a systematic review. *Neurol Therapy* 2019;8(2):351–65.
- [24] Yin W, Li L, Wu F-X. Deep learning for brain disorder diagnosis based on fMRI images. *Neurocomputing* 2022;469:332–45.
- [25] Guo H, Cheng C, Cao X, Xiang J, Chen J, Zhang K. Resting-state functional connectivity abnormalities in first-onset unmedicated depression. *Neural Regeneration Res* 2014;9(2):153.
- [26] Kim J, Calhoun VD, Shim E, Lee J-H. Deep neural network with weight sparsity control and pre-training extracts hierarchical features and enhances classification performance: Evidence from whole-brain resting-state functional connectivity patterns of schizophrenia. *Neuroimage* 2016;124:127–46.
- [27] Bronstein MM, Bruna J, LeCun Y, Szlam A, Vandergheynst P. Geometric deep learning: going beyond euclidean data. *IEEE Signal Process Mag* 2017;34(4):18–42.
- [28] Scarselli F, Gori M, Tsoi AC, Hagenbuchner M, Monfardini G. The graph neural network model. *IEEE Trans Neural Netw* 2008;20(1):61–80.
- [29] Zhou J, Cui G, Hu S, Zhang Z, Yang C, Liu Z, et al. Graph neural networks: A review of methods and applications. *AI Open* 2020;1:57–81.
- [30] Fout A, Byrd J, Shariat B, Ben-Hur A. Protein interface prediction using graph convolutional networks. *Adv Neural Inf Process Syst* 2017;30.
- [31] Rhee S, Seo S, Kim S. Hybrid approach of relation network and localized graph convolutional filtering for breast cancer subtype classification. 2017, arXiv preprint arXiv:1711.05859.
- [32] Do K, Tran T, Venkatesh S. Graph transformation policy network for chemical reaction prediction. In: *Proceedings of the 25th ACM SIGKDD international conference on knowledge discovery & data mining*. 2019, p. 750–60.
- [33] Qu G, Hu W, Xiao L, Wang J, Bai Y, Patel B, et al. Brain functional connectivity analysis via graphical deep learning. *IEEE Trans Biomed Eng* 2021;69(5):1696–706.
- [34] Battaglia P, Pascanu R, Lai M, Jimenez Rezende D, et al. Interaction networks for learning about objects, relations and physics. *Adv Neural Inf Process Syst* 2016;29.
- [35] Hoshen Y. Vain: Attentional multi-agent predictive modeling. *Adv Neural Inf Process Syst* 2017;30.
- [36] Rolls ET, Huang C-C, Lin C-P, Feng J, Joliot M. Automated anatomical labelling atlas 3. *Neuroimage* 2020;206:116189.
- [37] Bastos AM, Schoffelen J-M. A tutorial review of functional connectivity analysis methods and their interpretational pitfalls. *Front Syst Neurosci* 2016;9:175.
- [38] Giusti C, Ghrist R, Bassett DS. Two's company, three (or more) is a simplex. *J Comput Neurosci* 2016;41(1):1–14.
- [39] Huang W, Rong Y, Xu T, Sun F, Huang J. Tackling over-smoothing for general graph convolutional networks. 2020, arXiv preprint arXiv:2008.09864.
- [40] Li Q, Han Z, Wu X-M. Deeper insights into graph convolutional networks for semi-supervised learning. In: *Thirty-second AAAI conference on artificial intelligence*. 2018.
- [41] Zeng L-L, Shen H, Liu L, Hu D. Unsupervised classification of major depression using functional connectivity MRI. *Hum Brain Mapp* 2014;35(4):1630–41.
- [42] Zeng L-L, Shen H, Liu L, Wang L, Li B, Fang P, et al. Identifying major depression using whole-brain functional connectivity: a multivariate pattern analysis. *Brain* 2012;135(5):1498–507.
- [43] Li Y, Dai X, Wu H, Wang L. Establishment of effective biomarkers for depression diagnosis with fusion of multiple resting-state connectivity measures. *Front Neurosci* 2021;975.